

EXTENDED EXPERIMENTAL PROCEDURES

Material

The transgenic lines used have been described previously: *HS::axr3-1* (Knox et al., 2003); *tir1/afb1/afb2/afb3* (Dharmasiri et al., 2005a); RabF2b-YFP, RabC1-YFP, VTI12-YFP and RabA1g-YFP (Geldner et al., 2009); CLC-GFP (Konopka et al., 2008); *snx1-1* (Jailais et al., 2006); *axr3-1* (Rouse et al., 1998); *axr2-1* (Nagpal et al., 2000); 35S(2x)::miRNA160 (Wang et al., 2005); *vps29-3* (Kleine-Vehn et al., 2008); *abp1* knockdown lines (SS12S, SS12K and AS; Braun et al., 2008); *DR5::GUS* (Ulmasov et al., 1997); *pin1-1* (Okada et al., 1991); *eir1-1* (Luschig et al., 1998); and *DR5rev::GFP* (Friml et al., 2003). The *abp1-5* mutant, provided by the ABRC stock center (#CS91358), led to a change of a highly conserved histidine to a tyrosine (H94Y) in the BOX A of the ABP1 protein. *abp1-5* had been backcrossed 5 times with Col-0 and genotyped by restriction digestion of PCR fragments (primers: Atabpe1x2FW 5'-TGACCTTCCT-CAGGATAACTATGG-3' and Atabp1ex4RV 5'-CCAACACCTGCAGGTCCTCATGAC-3'). A restriction fragment length polymorphism upon *RsaI* digestions allowed identification of *abp1-5*. Three fragments were generated in wild-type (523, 207, and 73 bp) whereas four fragments were observed in *abp1-5* (523, 165, 73, and 45 bp).

The inducible HUB line was constructed with pINTAM and dominant negative HUB with the GAL4/UAS-based transactivation system (Dhonukshe et al., 2007). *HUB* expression was induced on solid media containing 2 μ M 2-hydroxytamoxifen for the time indicated. ABP1-GFP was cloned by inserting GFP into ABP1 after the glycine 120 by primer extension PCR with one or two glycines flanking the GFP coding sequence, respectively. 35S::ABP1-GFP functionality was tested by complementation of *abp1/abp1*. The 35S::ABP1 ^{Δ KDEL}-GFP construct was made based on the aforementioned primers, replacing the C-terminal KDEL motif of ABP1 with a stop codon. Similarly, ABP1-5 ^{Δ KDEL} was cloned by amplifying ABP1 from *abp1-5* lacking the KDEL ER retention motif.

In Situ Visualization of Auxin-Induced Gene Expression

Four-day-old *DR5rev::GFP* or *DR5::GUS* seedlings were transferred to sterile 0.5 MS liquid medium supplemented with either 5 or 25 μ M of the analyzed compounds and incubated for 3 hr. The compounds tested were 5-chloro-indole-3-acetic acid (5-Cl-IAA), 5-bromo-indole-3-acetic acid (5-Br-IAA), indole-3-carboxylic acid (I3CA), 4-chloro-indole-3-acetic acid (4-Cl-IAA), purchased from OlChemim Ltd. (http://www.olchemim.cz/INDEX_e.HTM), indole-3-acetic acid (IAA), 5-fluoroindole-3-acetic acid (5-F-IAA), 6-chloro-indole-3-acetic acid (6-Cl-IAA), naphthalene-1-acetic acid (1-NAA), naphthalene-2-acetic acid (2-NAA), naphthalene, indole, phenyl acetic acid (PAA), indole-3-butyric acid (IBA), 2,4-dichloro-phenoxy acetic acid (2,4-D), 2,4,5-trichloro-phenoxy acetic acid (2,4,5-T), 2,4-dichloro-phenoxy propionic acid (2,4-DP), indole-3-acetyl-L-alanine (IAA-L-Ala), indole-3-propionic acid (IPA), benzoic acid (BA), indole-3-lactic acid (ILA) (Sigma, <http://www.sigmaaldrich.com/>) and α -(phenyl ethyl-2-one)-indole-3-acetic acid (PEO-IAA) (Hayashi et al., 2008).

Synthesis of PEO-IAA

PEO-IAA was synthesized by the nucleophilic addition of indole to trans-3-benzoylacrylic acid using essentially the same reaction procedure as in (Abubshait SA, 2007). Briefly, equal moles of indole and trans-3-benzoylacrylic acid were refluxed in benzene for 12 hr. The crude solid was precipitated after cooling on ice, and then recrystallized from benzene to give pure PEO-IAA as colorless crystal (79% Yield): m.p. 149–150°C; IR ν max: 3400, 3055, 1711, 1677, 1453 cm^{-1} ; ^1H NMR (400 MHz, acetone- d_6): δ 3.41(1H, dd, J = 17.8, 4.1 Hz), 4.13(1H, dd, J = 17.8, 11.0 Hz), 4.57(1H, dd, J = 11.0, 4.1 Hz), 7.06(1H, t, J = 8.2 Hz), 7.13(1H, t, J = 8.2 Hz), 7.37(1H, s), 7.41(1H, d, J = 8.2 Hz), 7.51(2H, dd, J = 8.2, 7.8 Hz), 7.57(1H, t, J = 7.8 Hz), 7.80(1H, d, J = 8.3 Hz), 8.05(2H, d, J = 8.2 Hz), 10.17(1H, brs, COOH); ^{13}C NMR (100 MHz, acetone- d_6): δ 38.51, 42.35, 112.27, 113.35, 119.78, 119.94, 122.36, 123.72, 127.41, 128.72, 129.36, 133.80, 137.58, 137.66, 175.48, 198.71; FAB-MS: m/z 294 $[\text{M}+\text{H}]^+$; HRFAB-MS: m/z 294.1143 $[\text{M}+\text{H}]^+$, calcd. for 294.1130 ($\text{C}_{18}\text{H}_{16}\text{NO}_3$).

Transient Transformation of Tobacco BY-2 Cells

Ten ml of 3-day-old cells were harvested on filter paper by vacuum filtration and kept on solid BY-2 medium. The cells were transformed via particle bombardment with a PDS-1000/He biolistic system (Biorad) according to the manufacturer's recommendations. To coat the gold particles with DNA, 2 μ l of plasmid DNA (0.05 $\mu\text{g}/\mu\text{l}$ of each construct to transform) was added to 6.25 μ l of 1.6- μm diameter gold particles and the suspension was supplemented with 2.5 μ l spermidine (0.1 M stock solution) and 6.25 μ l CaCl_2 (2.5 M stock solution). The particles were pelleted by centrifugation, washed twice with 70% and 100% ethanol. The pellet was suspended in 10 μ l of 100% ethanol. Cells were bombarded under a pressure of 1100 psi. After transformation, 1 ml of auxin-free medium (mock) or enriched with 10 μM NAA or 10 μM 5-F-IAA was added to the cells. The plates were sealed with parafilm and kept in darkness for 18 hr at 25°C. Samples were analyzed via confocal microscopy (Zeiss 710).

Quantification of FM4-64 Uptake

The mean fluorescence intensity of vesicles inside the cell excluding the plasma membrane was measured with the ImageJ software (National Institutes of Health, <http://rsb.info.nih.gov/ij/>). Quotients of intracellular and plasma membrane fluorescence intensities were calculated for 10 to 15 cells from at least three different roots. The average of three independent experiments was calculated. The value of each phenotype was standardized to corresponding wild-type controls. SS12S and SS12K *abp1* knockdown lines were

induced for 24 hr before measurements with an 8% ethanol solution kept in a vial at the bottom of vertically oriented plates (Braun et al., 2008). Data were analyzed by Student's t test (http://www.physics.csbsju.edu/stats/t-test_bulk_form.html).

Quantitative RT-PCR

Total RNA was extracted with the RNeasy kit (QIAGEN). Poly(dT) cDNA was prepared from total RNA with Superscript III (Invitrogen). Quantitative RT-PCR was done with LightCycler 480 SYBR Green I Master reagents (Roche Diagnostics) and a LightCycler 480 Real-Time PCR System (Roche Diagnostics). Targets were quantified with specific primer pairs designed with Beacon Designer 4.0 (Premier Biosoft International). Data were analyzed with qBASE v1.3.4 (Hellemans et al., 2007). Expression levels were normalized to the non-auxin-responsive genes *PEROXIN4* (At5g25760), *UBIQUITIN-SPECIFIC PROTEASE 8* (At5g22030) and an unknown protein (At4g16100). For primer sequences, see Table S1.

SUPPLEMENTAL REFERENCES

- Abubshait, S.A. (2007). An efficient synthesis and reactions of novel indolylpyridazinone derivatives with expected biological activity. *Molecules* 12, 25–42.
- Friml, J., Vieten, A., Sauer, M., Weijers, D., Schwarz, H., Hamann, T., Offringa, R., and Jürgens, G. (2003). Efflux-dependent auxin gradients establish the apical-basal axis of *Arabidopsis*. *Nature* 426, 147–153.
- Geldner, N., Anders, N., Wolters, H., Keicher, J., Kornberger, W., Müller, P., Delbarre, A., Ueda, T., Nakano, A., and Jürgens, G. (2003). The *Arabidopsis* GNOM ARF-GEF mediates endosomal recycling, auxin transport, and auxin-dependent plant growth. *Cell* 112, 219–230.
- Geldner, N., Dénervaud-Tendon, V., Hyman, D.L., Mayer, U., Stierhof, Y.-D., and Chory, J. (2009). Rapid, combinatorial analysis of membrane compartments in intact plants with a multicolor marker set. *Plant J.* 59, 169–178.
- Hayashi, K.-i., Tan, X., Zheng, N., Hatate, T., Kimura, Y., Kepinski, S., and Nozaki, H. (2008). Small-molecule agonists and antagonists of F-box protein-substrate interactions in auxin perception and signaling. *Proc. Natl. Acad. Sci. USA* 105, 5632–5637.
- Hellemans, J., Mortier, G., De Paepe, A., Speleman, F., and Vandesompele, J. (2007). qBase relative quantification framework and software for management and automated analysis of real-time quantitative PCR data. *Genome Biol.* 8, R19.
- Jaillais, Y., Fobis-Loisy, I., Miège, C., Rollin, C., and Gaudé, T. (2006). AtSNX1 defines an endosome for auxin-carrier trafficking in *Arabidopsis*. *Nature* 443, 106–109.
- Luschnig C, Gaxiola RA, Grisafi P, Fink GR.(1998). EIR1, a root-specific protein involved in auxin transport, is required for gravitropism in *Arabidopsis thaliana*. *Genes Dev.* 12, 2175–2187.
- Nagpal, P., Walker, L.M., Young, J.C., Sonawala, A., Timpte, C., Estelle, M., and Reed, J.W. (2000). AXR2 encodes a member of the Aux/IAA protein family. *Plant Physiol.* 123, 563–574.
- Okada, K., Ueda, J., Komaki, M.K., Bell, C.J., and Shimura, Y. (1991). Requirement of the Auxin Polar Transport System in Early Stages of *Arabidopsis* Floral Bud Formation. *Plant Cell* 3, 677–684.
- Peyroche, A., Antonny, B., Robineau, S., Acker, J., Cherfils, J., and Jackson, C.L. (1999). Brefeldin A acts to stabilize an abortive ARF-GDP-Sec7 domain protein complex: involvement of specific residues of the Sec7 domain. *Mol. Cell* 3, 275–285.
- Rouse, D., Mackay, P., Stirnberg, P., Estelle, M., and Leyser, O. (1998). Changes in auxin response from mutations in an AUX/IAA gene. *Science* 279, 1371–1373.
- Wang, J.-W., Wang, L.-J., Mao, Y.-B., Cai, W.-J., Xue, H.-W., and Chen, X.-Y. (2005). Control of root cap formation by MicroRNA-targeted auxin response factors in *Arabidopsis*. *Plant Cell* 17, 2204–2216.
- Zeeh, J.-C., Zeghouf, M., Grauffel, C., Guibert, B., Martin, E., Dejaegere, A., and Cherfils, J. (2006). Dual specificity of the interfacial inhibitor brefeldin A for arf proteins and sec7 domains. *J. Biol. Chem.* 281, 11805–11814.

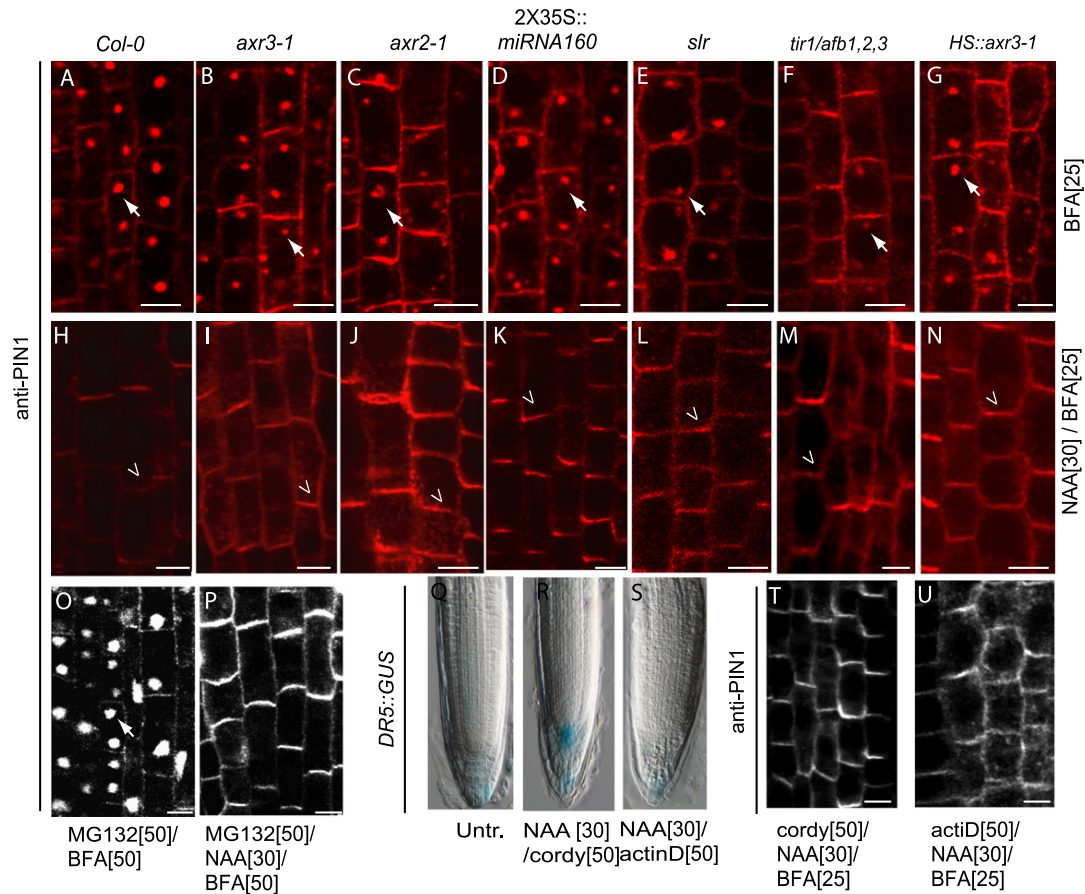


Figure S1. Aux/IAA-Independent Signaling for Auxin Effect on PIN Internalization, Related to Figure 1

(A–G) BFA-induced internalization of PIN1 in wild-type (A) and TIR1-Aux/IAA signaling-deficient transgenic seedlings: *axr3-1* (B), *axr2-1* (C), *2X35S::miRNA160* (D), *slr-1* (E), *tir1/afb1,2,3* (F) and *HS::axr3-1* (G).

(H–N) BFA-induced PIN accumulations inhibited by NAA (30 min pretreatment) in wild-type (H) and in TIR1-Aux/IAA signaling-deficient transgenic seedlings, such as *axr3-1* (I), *axr2-1* (J), *2X35S::miRNA160* (K), *slr-1* (L), *tir1/afb1,2,3* (M) and *HS::axr3-1* (N).

(O–T) Interference with MG132-dependent proteasome activity (O and P) and cordycepin- (Q and S) or actinomycin-dependent (R and T) transcription did not affect auxin effect on BFA-induced PIN internalization. After inhibition of the proteasome activity by MG132 for 30 min, cotreatment with BFA-induced PIN protein internalization (O) and the effect of auxin on PIN internalization still occurred (P). Upon incubation with the transcription inhibitors cordycepin and actinomycin D for 30 min, auxin did not induce the activity of auxin-responsive promoter *DR5rev::GFP* (Q–S), but still inhibited PIN protein internalization after 3 hr of treatment (T and U).

Arrows mark PIN proteins internalized in BFA compartments and arrowheads highlight PIN protein retention at the plasma membrane. Scale bar: 10 μ m.

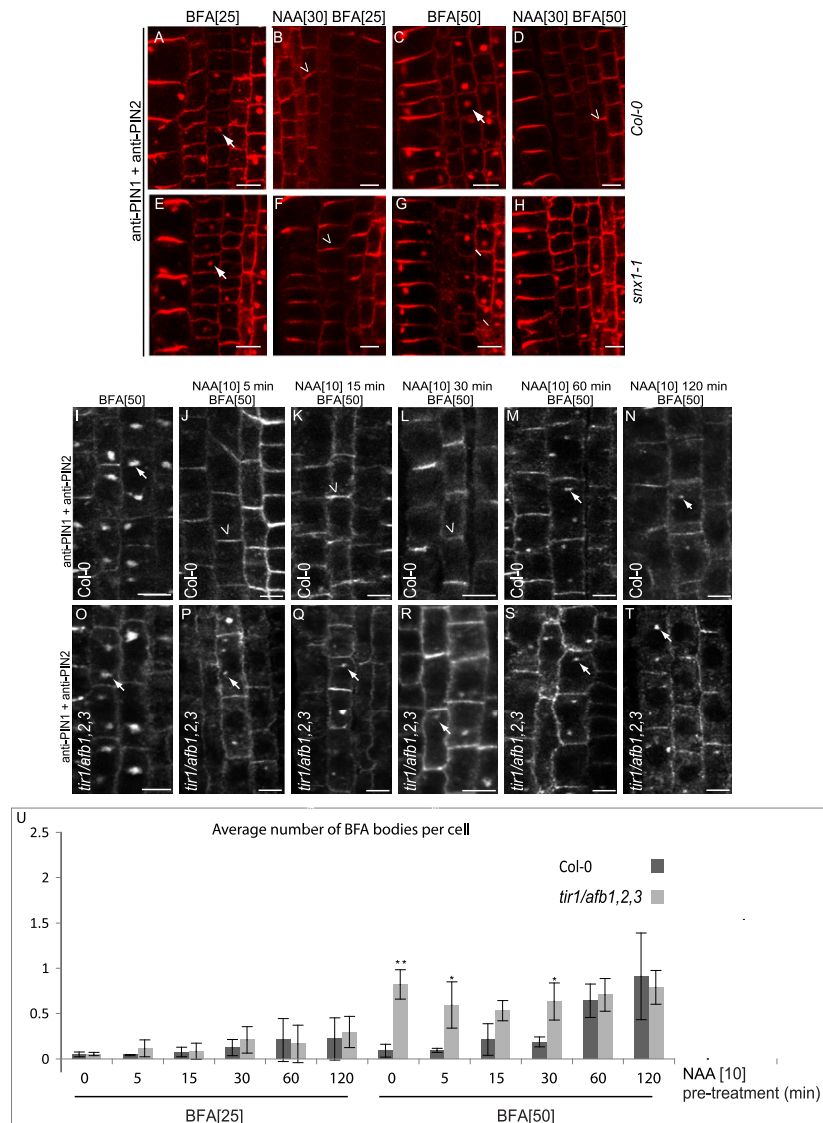


Figure S2. Auxin Effect on BFA-Induced PIN Internalization and Degradation, Related to Figure 2

BFA is a well-characterized inhibitor of a subclass of ARF-GEF, regulators of vesicle budding. BFA sensitivity of different ARF-GEFs depends on a single amino acid in the ARF-GEF sequence and the actual interacting ARF partner (Peyroche et al., 1999; Geldner et al., 2003; Zeeh et al., 2006). Thus, different ARF-GEF-mediated subcellular vesicle trafficking processes can show clear differences in BFA sensitivity. For instance, 25 μ M BFA appears to specifically interfere with the recycling processes to the plasma membrane, whereas 50 μ M BFA affects also the degradation pathway to the vacuole (Kleine-Vehn et al., 2008). Therefore we used this differential effect to distinguish the auxin effect on PIN internalization and PIN vacuolar targeting.

(A–H) Auxin effect on PIN internalization and degradation visualized by the presence or absence of PIN proteins in BFA bodies: NAA (30 min pretreatment) inhibited BFA-induced PIN1 and PIN2 intracellular accumulation at both 25 μ M and 50 μ M BFA in wild-type seedlings (A–D). In mutants with an increased PIN turnover in lytic vacuoles, such as *snx1-1* (Kleine-Vehn et al., 2008) (E–H), NAA prevented the BFA-induced PIN1 and PIN2 intracellular accumulation only at 25 μ M (E and F), but not at 50 μ M BFA (G and H), indicating that BFA treatment at 50 μ M visualizes PIN proteins that are designated for degradation, while BFA incubation at 25 μ M predominantly affects PIN recycling.

(I–T) Analysis of the effect of auxin (10 μ M) and BFA (50 μ M) cotreatment for PIN degradation over time in wild-type (I–N) and in a *tir1/afb* quadruple mutant (O–T). The rate of PIN protein turnover, as visualized by an increased accumulation of PIN proteins in 50 μ M BFA-induced compartments, was higher in the *tir1/afb* quadruple mutant than in the wild-type.

(U) Average number of BFA bodies per cell under the conditions described in Figure 2. $n = 3$ independent experiments with at least 60 cells counted for each assay. Error bars represent standard deviation. * and ** mark statistically significant p values at < 0.05 and < 0.001 , respectively.

Arrows mark PIN proteins internalized in BFA compartments and arrowheads highlight PIN protein retention at the plasma membrane. Scale bar: 10 μ m.

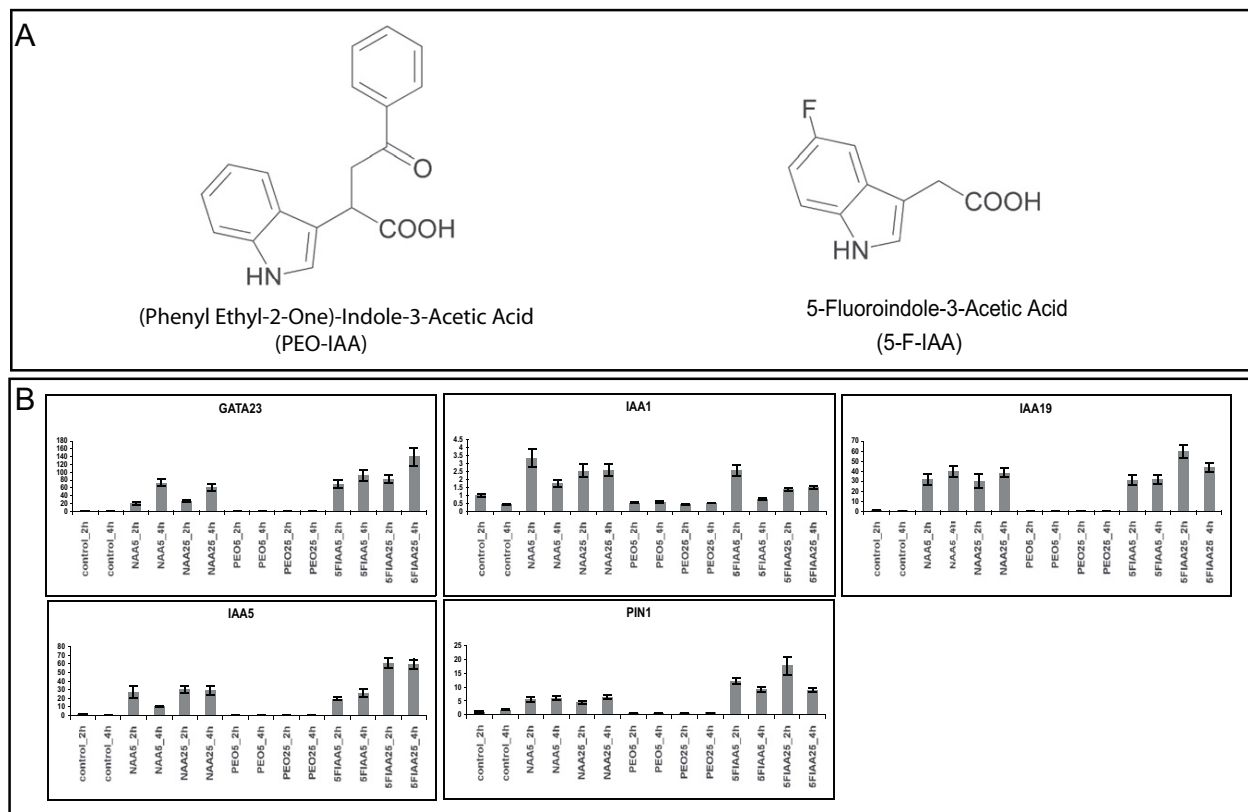


Figure S3. α -(Phenyl Ethyl-2-one)-Indole-3-Acetic Acid (PEO-IAA) and 5-Fluoro-IAA (5-F-IAA), Related to Figure 3

(A) Chemical structure of the auxin analogs PEO-IAA and 5-F-IAA.

(B) Effect of mock, NAA, PEO-IAA and 5-F-IAA on transcript levels of auxin-regulated genes, such as *GATA23*, *IAA1*, *IAA19*, *IAA5*, and *PIN1* at two different time points (2 hr and 4 h). Data were normalized to non-auxin responsive genes *PEROXIN4* (At5g25760), *UBIQUITIN-SPECIFIC PROTEASE 8* (At5g22030), and an unknown protein (At4g16100). Transcript levels of auxin-inducible genes were still responsive to 5-F-IAA, but not to PEO-IAA in accordance with Figure 3. Error bars represent standard deviation.

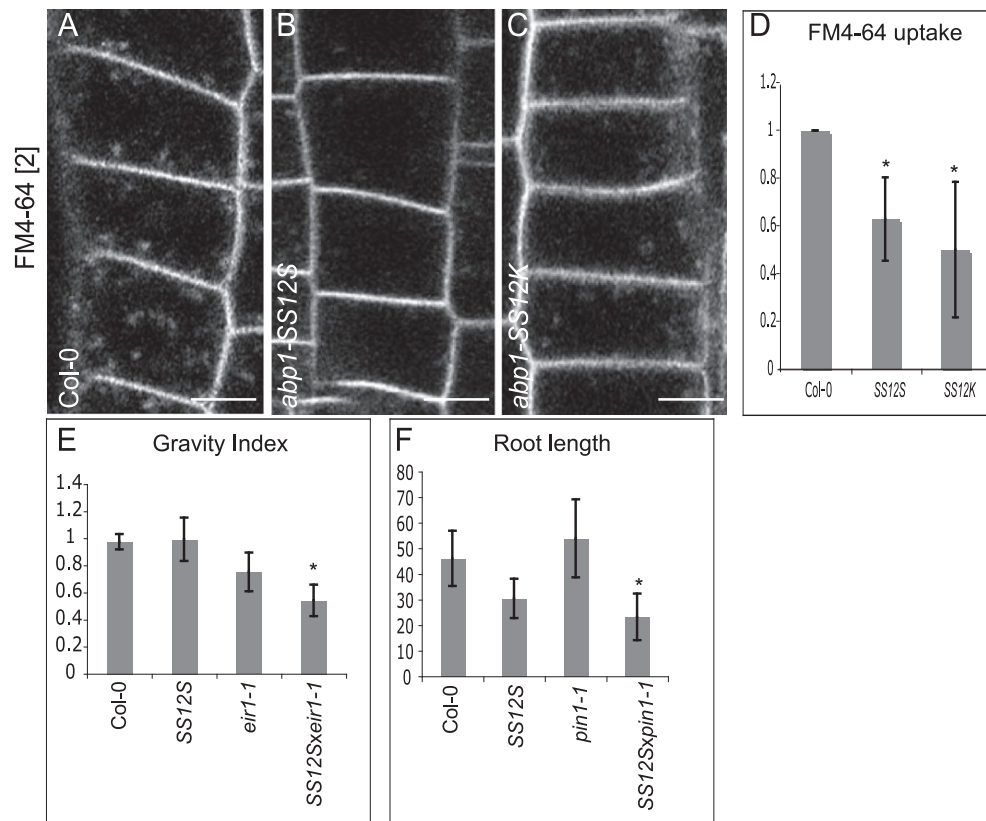


Figure S4. ABP1 Downregulation Inhibits Endocytosis, Related to Figure 4

(A–C) Inhibited uptake of the endocytotic tracer FM4-64 in the inducible *abp1* knock-down lines SS12S (B) and SS12K (C) when compared to the induced wild-type (A). Quantification of FM4-64 uptake in the wild-type and in conditional *abp1* knock-down lines (D). $n > 3$ independent experiments with at least 90 cells analyzed for each assay.

(E–F) Genetic interaction between an *abp1* knock-down line and *pin* mutants: defects in gravity responses of *eir1-1* (E) and in root elongation of *pin1-1* (F) were enhanced by *ABP1* downregulation. Measurements have been done on 7 to 40 roots for each assay.

Scale bar: 10 μm . Error bars represent standard deviation. * and ** mark statistically significant p values at < 0.05 and < 0.001 , respectively.

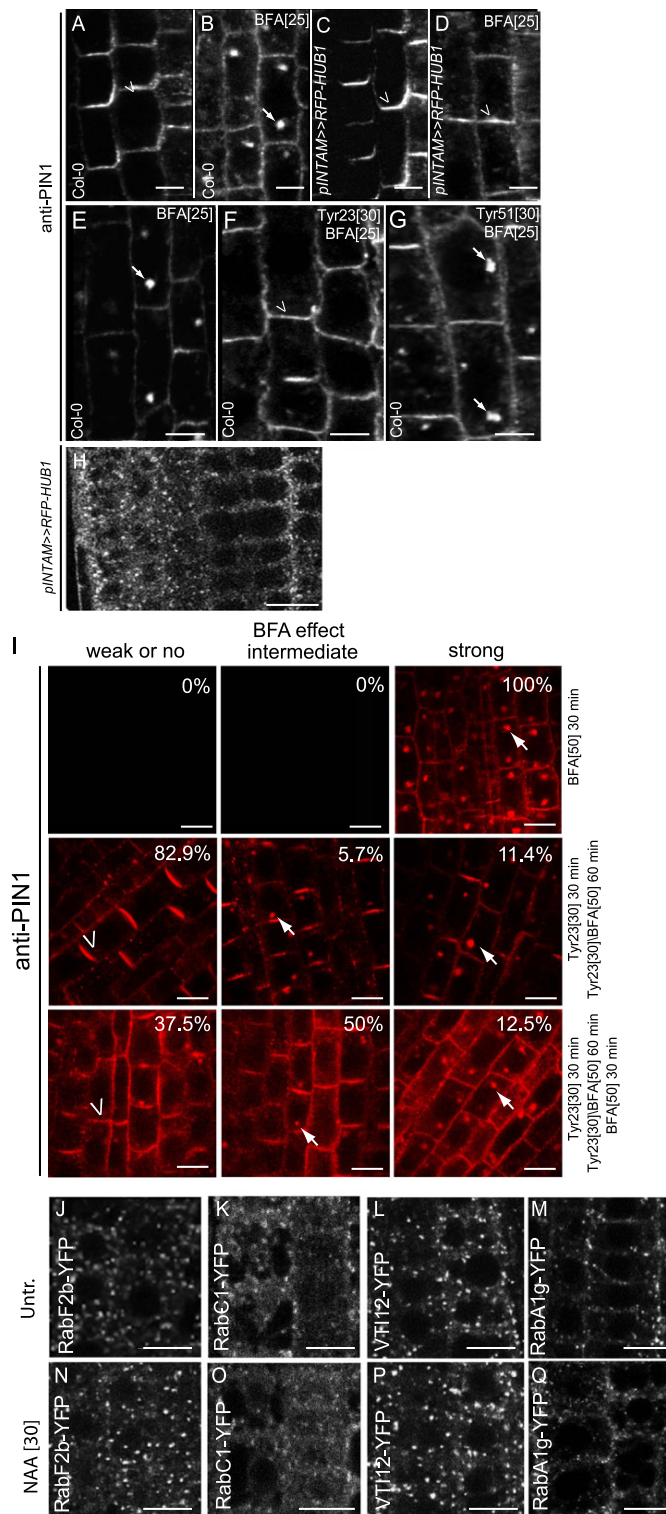


Figure S5. PIN Proteins Internalized through a Clathrin-Dependent Pathway, Related to Figure 6

Elevated HUB1 levels tagged with red fluorescent protein (RFP) in inducible *pINTAM >> RFP-HUB1* lines correlate with reduced PIN internalization upon BFA treatment.

(A–D) PIN1 localization in non-induced (A and B) and induced for 30 hr (C and D) dominant-negative clathrin HUB1 lines: BFA-induced PIN1 internalization (B) was inhibited by HUB1 induction (D).

(E–G) BFA-induced PIN1 internalization (E) was inhibited by tyrphostin A23 (30 min pretreatment) (F), but not by the inactive analog tyrphostin A51 (G).

(H) Visualization of pINTAM > > RFP-HUB after induction with 2 μ M tamoxifen for 12 hr. Arrows mark PIN proteins internalized into BFA compartments and arrowheads PIN protein retention at the plasma membrane.

(I) BFA-induced PIN1 internalization (top): tyrphostin A23, when applied prior to BFA, strongly reduced the BFA-induced PIN internalization (middle). This effect was reversible when tyrphostin A23 was removed and replaced by BFA for another 30 min (bottom).

(J–Q) Auxin treatment (30 min) did not affect localization of RabF2b (J and N), RabC1 (K and O), VTI12 (L and P) and RabA1g (M and Q) fused to yellow fluorescent protein (YFP). Arrows mark PIN proteins internalized in BFA compartments and arrowheads highlight PIN protein retention at the plasma membrane. Scale bar: 10 μ m.

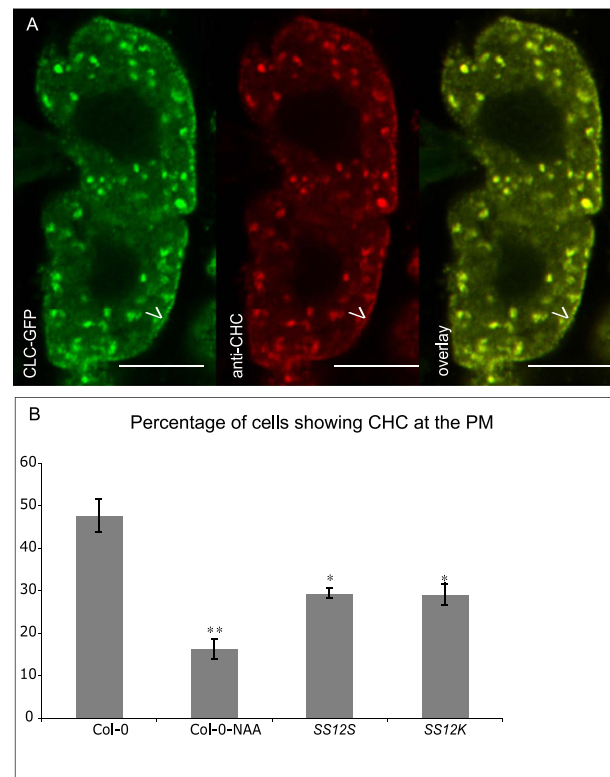


Figure S6. Auxin Affects Clathrin Heavy Chain, but Not Other Endosomal Regulators, Related to Figure 7

(A) Co-localization of a CLC-GFP fusion protein with immunodetected CHC. Seedlings expressing *CLC::CLC:GFP* were used for immunolabeling with an anti-CHC antibody (detected with Cy3 secondary antibody). Signals detected upon excitation with either 488 nm (GFP, in green) or 561 nm (Cy3, in red) indicated pronounced protein co-localization (see overlay). Arrowheads show clathrin at the plasma membrane. Scale bar: 10 μ m. Error bars represent standard deviation. * and ** mark statistically significant p values at < 0.05 and < 0.001, respectively.

(B) Quantification CHC at the plasma membrane in wild-type and *abp1* knock-down lines upon auxin-treatment for 30 min or in untreated controls. Percentage of cells per root displaying CHC localized to the plasma membrane. $n = 3$ independent experiments with at least 90 cells analyzed for each assay. Arrowheads show clathrin at the plasma membrane. Scale bar: 10 μ m. Error bars represent standard deviation. * and ** mark statistically significant p values at < 0.05 and < 0.001, respectively.